SECONDARY FREQUENCY REGULATION CHARACTERISTIC MODELING OF THERMAL POWER UNITS BASED ON BOUNDED-GAIN-FORGETTING METHOD

Xiufeng XING[1], Fengsheng JIA[1], Xinglei YAN[1], Jian LV[1], Honghai LI[2,*]

The existing mechanism models for thermal power units face challenges in accurately reflecting unit response characteristics under different working conditions. To address this, this paper proposes a novel modeling method for the secondary frequency regulation characteristics of thermal power units. The frequency regulation response characteristics of Automatic Generation Control (AGC) are firstly analyzed from the historical operating data, and then it is concluded that a second-order model can represent the unit's response characteristics under a step power command. Next, the Bounded-Gain-Forgetting (BGF) algorithm is improved to identify the parameters in this second-order model adaptively. Interestingly, the proposed method is also suitable to the case where the model parameters vary caused by the change of working conditions, thereby enhancing the model's adaptability to the actual unit response. Finally, case studies are designed to verify the effectiveness and superiority of the proposed model.

Keywords: Thermal power unit, secondary frequency regulation characteristic, automatic generation control, Bounded-Gain-Forgetting.

1. Introduction

In recent years, the installed capacity of new energy sources such as wind power and photovoltaic power in China has been rising continuously, and it is expected that their installed capacity will exceed that of thermal power by 2035 [1-2]. While the proportion of new energy in the power generation structure is increasing, it has also brought severe challenges to the power balance of the power system. This is mainly because new energy sources with a high proportion of integration have significant intermittency and volatility, which are prone to generate rapidly changing power fluctuation components [3]. To improve the absorption capacity of new energy and maintain the stability of the power system, it is necessary to rely on thermal power units to regulate the power system [4].

Power grid frequency regulation mainly includes primary frequency regulation, secondary frequency regulation, and tertiary frequency regulation [5]. Primary frequency regulation is realized by the governor of synchronous generators

[1] Shanxi Century Pilot Electric Power Science and Technology Co., Ltd., Taiyuan, Shanxi, 030012, China
[2] Shandong Luruan Digital Technology Co., Ltd., Jinan, Shandong, 250002, China
[*] E-mail: honghai_1402@163.com

and can adapt to small load fluctuations in a short period. Secondary frequency regulation (SFR), achieved through Automatic Generation Control (AGC), is a feedback process that maintains grid stability by adjusting generator output in response to load fluctuations. Tertiary frequency regulation is performed by Economic Dispatch Control (EDC), which calculates the most economical output for each generating unit based on historical load fluctuations and predictions of future demand, and then dispatches these optimized set points as control commands to the respective power plants for execution [6]. This paper focuses on the secondary frequency regulation, and it is noted that poor secondary frequency regulation performance is difficult to fully meet the requirements of the new power system for frequency stability, due to their slow adjustment response speed and low efficiency [7-8]. Significant research has been dedicated to SFR. Specifically, Zhang et al. [9] introduced a distributed control strategy based on an enhanced tie-line bias scheme, rigorously proving its stability under communication delays via Lyapunov analysis. To address photovoltaic uncertainty, Fang et al. [10] developed a distributionally robust optimization framework to enhance the reliability of renewable-based regulation. Furthermore, Wen et al. [11] proposed a joint optimization model coordinating battery energy storage systems (BESS) with synchronous units, where BESS provides fast frequency response to mitigate fluctuations caused by high renewable penetration. In addition, deep reinforcement learning was employed by Zhang et al. [12] for the flexible selection and multi-objective optimization of SFR units. The efficacy of these strategies, however, hinges on a precise understanding of the participating units' dynamic characteristics—particularly the time-varying parameters of thermal power plants. Consequently, establishing accurate and adaptive mechanism models for thermal units is crucial for optimizing response performance [13-15] and has become an urgent operational necessity.

Existing research on frequency regulation modeling for thermal power units has specific limitations. Sun et al. [16] optimized the governor model for primary frequency regulation by developing a coupling function and dynamic model for valve flow and main steam pressure. Zhang et al. [17] differentiated the control processes of primary and secondary frequency regulation by analyzing the second-derivative of their response power, enabling separate performance evaluations. Nonetheless, a dedicated and accurate mechanism model for secondary frequency regulation is still lacking. Another study [18] examined boiler heat storage's effect on grid frequency during peak shaving but used a simplified boiler model with condition-sensitive parameters. Although Cao et al. [19] derived useful sensitivity functions by modeling generator, governor, and turbine dynamics, their model's linearized approach cannot fully represent actual nonlinear unit responses. Note that the secondary frequency regulation process of thermal power units is complex and moreover, in the actual operation process, parameters may change in real time with operating conditions and working fluids [20-22]. As a result, it is difficult to construct an accurate mechanism model and identify precise model parameters for secondary frequency regulation. Therefore, it is necessary to develop an adaptive parameter identification algorithm to update the model parameters automatically.

This paper proposes a novel adaptive modeling and identification framework for the secondary frequency regulation characteristics of thermal power units. Our work makes three key contributions that address critical gaps in existing methodologies:

- Refining SFR Modeling: Based on operational data analysis, we demonstrate for the first time that the AGC response of thermal units under step commands is accurately characterized by a second-order system. This provides a dedicated online identification model that captures core inertial and damping dynamics—essential features often overlooked by existing mechanistic models, which typically focus on primary frequency regulation or rely on oversimplified linear approximations.
- Algorithmic Innovation: An improved Bounded-Gain-Forgetting (BGF) algorithm is introduced for online parameter identification to address time-varying dynamics under fluctuating operating conditions. Unlike standard least-squares (LS) methods, this adaptive scheme effectively tracks parameter variations in non-stationary environments, ensuring robust model adaptation.
- Empirical Validation and Utility: The proposed framework is rigorously validated using real-world operational data across diverse regulation scenarios (varying amplitudes and directions). The results demonstrate superior accuracy and adaptability compared to conventional fixed-parameter models, establishing a robust foundation for the design and optimization of coordinated thermal-storage AGC systems.

The paper is organized as follows: In Section 2, secondary frequency regulation response characteristics are analyzed and modeled as a second-order system which will be further transformed to facilitate the parameter identification. Parameter identification algorithm is introduced in Section 3 and simulation validation is conducted in Section 4. And then conclusions are drawn in Section 5.

2. Analysis of Secondary Frequency Regulation Response Characteristics

Fig.1 illustrates the dynamic variation process of AGC power commands p^* and the actual power output p from a 330 MW thermal power unit within a specific time period. From Fig.1, it can be seen that when the power command p^* changes in a stepwise manner, the actual power output p of the unit does not respond instantaneously. Instead, it firstly undergoes a short delay and then tracks the command in a pattern of rapidly approaching and then converging with slight oscillations [23].

Fig.2 illustrates the typical response process to track an AGC command in the secondary frequency regulation. In Fig.2, P_{AGC} represents the AGC command that the unit needs to track, given at the moment T_0, and P_1 denotes the output of the thermal power unit at $t = T_0$. P_{min} and P_{max} refer to the regulation ranges of the thermal power unit. The time interval from T_1 to T_2 corresponds to the ramping phase of the thermal power unit in the process of responding to the AGC command, and the interval from T_2 to T_3 represents the stable phase of the unit during its response to the AGC command. Additionally, the interval from T_0 to T_1 reflects the response time to the AGC command of the thermal power unit [7].

From the characteristics shown in Fig.1 and Fig.2, it is concluded that the trajectory change of the actual power output is consistent with the typical characteristics of a second-order system, which has inertial links and damping characteristics and is accompanied by overshoot or oscillation trends during response.

Fig. 1 The AGC command and the actual power output curve of a 330MW thermal power unit

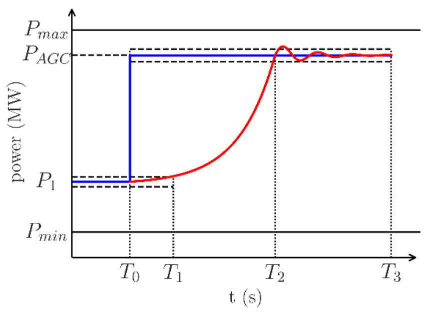

Fig. 2 Typical AGC response process under a step power command

It should be noted, the AGC system of thermal power units involves several critical nonlinear and operational factors, such as deadbands, ramping rate limits, and boiler-turbine coordinated control strategies. The deadband can cause the unit to be unresponsive to very small AGC commands. To circumvent this problem, large-magnitude step AGC command response data segments from units operating in the prevalent "Boiler-Follow" mode are selected, ensuring that the established second-order linear model accurately captures the core inertial and damping characteristics of the unit's secondary frequency regulation process. Ramping rate limit, a critical performance indicator strictly regulated by grid codes, is generally set to a sufficiently high value by power plants to meet dispatch demands. Hence, it is often not the dominant factor limiting the dynamic response during normal AGC operation. Regarding control strategies, the "Boiler-Follow" mode is extensively employed for its fast load response characteristics. In this mode, the turbine leads the power change while the boiler quickly follows, making it well-suited for providing AGC service.

2.1 Secondary Frequency Regulation Model for Thermal Power Units

From the analysis above, it is known that the secondary frequency regulation process of the thermal power unit can be modeled as a typical second-order system. Therefore, denote the actual power of AGC as $p(t)$, and the power command as $p^*(t)$, and their Laplace transformations are $P(s)$ and $P^*(s)$ respectively. Then the transfer function from power command $P^*(s)$ to actual power $P(s)$ is given by

$$\frac{P(s)}{P^*(s)} = \frac{\omega_n^2}{s^2 + 2\xi\omega_n s + \omega_n^2} \tag{1}$$

where ω_n is the natural frequency of the unit and ξ is the damping ratio of the unit.

The second-order system can change its response characteristics by modifying the damping ratio online. From the AGC command response characteristics shown in Fig.1 and Fig.2, the second-order system (1) with different damping ratios ξ is adopted to reflect different secondary frequency modulation response characteristics of the thermal power unit under varying operating conditions. Therefore, the aim is to develop a parameter identification algorithm to estimate different damping ratio ξ and give the power prediction.

2.2 Model transformation

In this section, some transformations are conducted for the second-order model (1) to facilitate the parameter identification.

Define

$$\begin{aligned} A(s) &= s^2 + a_1 s + a_0, a_1 = 2\xi\omega_n, a_0 = \omega_n^2 \\ A_0(s) &= s^2 + \alpha_1 s + \alpha_0, \alpha_1 = 2\xi_0\omega_{n0}, \alpha_0 = \omega_{n0}^2 \\ B(s) &= a_0 \end{aligned} \tag{2}$$

where ω_{n0} is the nominal natural frequency determined based on experiences and relevant technical data of the system and ξ_0 is the specified nominal damping ratio. Then (1) can be rewritten as

$$\begin{aligned} P(s) &= \frac{A_0(s)-A(s)}{A_0(s)}P(s)+\frac{B(s)}{A_0(s)}P^*(s) \\ &= \frac{(\alpha_1-a_1)sP(s)+(\alpha_0-a_0)P(s)}{A_0(s)}+\frac{a_0}{A_0(s)}P^*(s) \end{aligned} \tag{3}$$

Let $\theta^T=[\alpha_1-a_1,\alpha_0-a_0,a_0],\omega^T(t)=\left[\frac{s}{A_0(s)}p(t),\frac{1}{A_0(s)}p(t),\frac{1}{A_0(s)}p^*(t)\right]$,

then (3) can be further written as

$$p(t)=\theta^T\omega(t) \tag{4}$$

In the model (4), θ is the parameter vector which will be identified later, $\omega(t)$ denotes the information available which can be calculated from the historical data of the actual power and power command measurements.

In the following, we will show the algorithm how to get $\omega(k)$ from $p(i)$ and $p^*(i), i=0,1,\cdots,k$, where we substitute $\omega(k)$ for $\omega(kT)$ with T being the sampling period. Denote $\omega_1(t)=\frac{s}{A_0(s)}p(t)$, $\omega_2(t)=\frac{1}{A_0(s)}p(t)$ and $\omega_3(t)=\frac{1}{A_0(s)}p^*(t)$, and then $\omega(t)=[\omega_1(t)\quad\omega_2(t)\quad\omega_3(t)]^T$. Here take $\omega_1(t)$ as an example to illustrate the algorithm details. From (2), it follows

$$(s^2+\alpha_1 s+\alpha_0)\omega_1(t)=sp(t) \tag{5}$$

whose differential equation form is given by

$$\ddot{\omega}_1(t)+\alpha_1\dot{\omega}_1(t)+\alpha_0\omega_1(t)=\dot{p}(t) \tag{6}$$

Using Backward Difference Method, we have

$$\begin{aligned} \dot{\omega}_1(k) &= \frac{\omega_1(k)-\omega_1(k-1)}{T} \\ \dot{p}(k) &= \frac{p(k)-p(k-1)}{T} \end{aligned} \tag{7}$$

and

$$\ddot{\omega}_1(k)=\frac{\dot{\omega}_1(k)-\dot{\omega}_1(k-1)}{T} \tag{8}$$

Substitute (7) into (8) to get

$$\ddot{\omega}_1(k) = \frac{\omega_1(k)+\omega_1(k-2)-2\omega_1(k-1)}{T^2} \tag{9}$$

Substitute (7) and (9) into (6) and let $t=k$, and it follows that

$$\omega_1(k)=\frac{1}{1+\alpha_1 T+\alpha_0 T^2}(T(p(k)-p(k-1))-\omega_1(k-2)+(2+\alpha_1 T)\omega_1(k-1)) \tag{10}$$

Similarly, we have

$$\omega_2(k)=\frac{1}{1+\alpha_1 T+\alpha_0 T^2}(T^2 p(k)-\omega_2(k-2)+(2+\alpha_1 T)\omega_2(k-1)) \tag{11}$$

and

$$\omega_3(k)=\frac{1}{1+\alpha_1 T+\alpha_0 T^2}(T^2 p^*(k)-\omega_3(k-2)+(2+\alpha_1 T)\omega_3(k-1)) \tag{12}$$

3. Parameter Identification of Secondary Frequency Regulation Model

Denote $\hat{\theta}$ as the estimate of parameter vector θ, and $\hat{p}(t)$ as the corresponding power estimate, then

$$J=\int_0^t \| p(\tau)-\hat{\theta}^T\omega(\tau)\|^2 d\tau \tag{13}$$

Formula (13) is the thermal power prediction model which describes the secondary frequency regulation response characteristics for thermal power unit, as shown in Fig.3. To obtain the power prediction $\hat{p}(t)$, a parameter identification unit needs to be firstly designed to obtain $\hat{\theta}$. Therefore, in this section, the parameter identification algorithm for $\hat{\theta}$ will be studied.

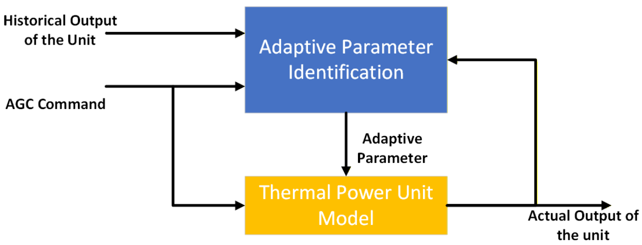

Fig. 3 Schematic diagram of the secondary frequency modulation response characteristic model for thermal power units

3.1 Parameter Identification based on standard least squares method

Standard least squares (LS) is a common and effective method for parameter identification. For the standard LS method, the performance index is defined as:

$$J=\int_0^t \| p(\tau)-\hat{\theta}^T\omega(\tau)\|^2 d\tau \tag{14}$$

To find $\hat{\theta}$ so as to minimize J in (14), it is required that $\frac{\partial J}{\partial \hat{\theta}}=0$ and then it follows

$$\hat{\theta}(t) = T(t)\int_0^t \omega(\tau)p(\tau)d\tau \tag{15}$$

and

$$\frac{d}{dt}[T^{-1}(t)] = \omega(t)\omega^T(t) \tag{16}$$

Differentiate (15) once to get $\dot{\hat{\theta}} = -T(t)\omega^T(t)e(t)$ where $e(t) = \hat{p}(t) - p(t)$. From (16), it follows $\dot{T}(t) = -T\omega(t)\omega^T(t)T$.

Proposition 1 If the parameter vector θ is constant and

$$\lambda_{min}\{\int_0^t \omega\omega^T dr\} \to \infty \qquad as \qquad t \to \infty \tag{17}$$

where $\lambda_{min}\{\cdot\}$ is the minimum eigenvalue, then $\hat{\theta} \to \theta$.

Proof 1

Integrate (16) from 0 to t and get

$$T^{-1}(t) = T^{-1}(0) + \int_0^t \omega(r)\omega^T(r)dr \tag{18}$$

Define $\tilde{\theta} = \hat{\theta} - \theta$ and differentiate $\tilde{\theta}$ once to obtain $\dot{\tilde{\theta}} = \dot{\hat{\theta}} = -T(t)\omega^T(t)e(t)$ from which, it follows that

$$\frac{d}{dt}[T^{-1}(t)\tilde{\theta}] = \frac{d}{dt}[T^{-1}(t)]\tilde{\theta} + T^{-1}(t)\dot{\tilde{\theta}} = \omega(t)\omega^T(t)\tilde{\theta} - \omega^T(t)e(t) \tag{19}$$

Consider that $e = \hat{p} - p = \hat{\theta}^T\omega - \theta^T\omega = \tilde{\theta}^T\omega = \omega^T\tilde{\theta}$ and (19) is further written as $\frac{d}{dt}[T^{-1}(t)\tilde{\theta}(t)] = 0$. Therefore, $T^{-1}(t)\tilde{\theta}(t) = T^{-1}(0)\tilde{\theta}(0)$ and $\tilde{\theta}(t) = T(t)T^{-1}(0)\tilde{\theta}(0)$. From (16), it is known that $T(t) \to 0$ as $t \to \infty$ and also $\tilde{\theta}(t) \to 0$ as $t \to \infty$.

From the proof above, it is clear that the standard LS method will lose its effectiveness in the case where the parameter vector θ is varying not constant, which will be circumvented by the BGF method in the following Section.

3.2 Parameter Identification based on BGF method

A forget factor $\lambda(t)$ is introduced to the standard LS method, which is called Bound-Gain-Forget (BGF) method.

In the BGF method, the performance index is defined as

$$J = \int_0^t exp\left[-\int_\tau^t \lambda(r)dr\right] \| p(\tau) - \hat{\theta}^T(t)\omega(\tau)\|^2 d\tau \tag{20}$$

with $\lambda(t)$ determined by

$$\lambda(t) = \lambda_0 \left(1 - \frac{\| T(t) \|}{k_0} \right) \tag{21}$$

where $\lambda_0 > 0$ is the maximum forgetting rate, $\| T(0) \| \le k_0$.

To find $\hat{\theta}$ so as to minimize J in (20), it is required that $\frac{\partial J}{\partial \hat{\theta}} = 0$. From (20), we have

$$\frac{\partial J}{\partial \hat{\theta}} = \int_0^t exp\left[-\int_\tau^t \lambda(r)dr \right] (p(\tau) - \hat{\theta}^T(t)\omega(\tau))(-\omega^T(\tau))d\tau \tag{22}$$

Let $\frac{\partial J}{\partial \hat{\theta}} = 0$ in (22) and it follows

$$\int_0^t exp\left[-\int_\tau^t \lambda(r)dr \right] p(\tau)\omega^T(\tau)d\tau = \hat{\theta}^T(t) \int_0^t exp\left[-\int_\tau^t \lambda(r)dr \right] \omega(\tau)\omega^T(\tau)d\tau \tag{23}$$

which is differentiate once with respect to time and then

$$p(t)\omega^T(t) = \hat{\theta}^T(t)\omega(t)\omega^T(t) + \dot{\theta}^T(t)T^{-1}(t) \tag{24}$$

where

$$T^{-1}(t) = \int_0^t exp\left[-\int_\tau^t \lambda(r)dr \right] \omega(\tau)\omega^T(\tau)d\tau \tag{25}$$

From (24), the updating law of $\hat{\theta}$ is given by $\dot{\theta}(t) = -T(t)\omega(t)e(t)$ where $e(t) = \hat{\theta}^T(t)\omega(t) - p(t)$. Define $\tilde{\theta} = \hat{\theta} - \theta$, then $e(t)$ can be further written as

$$e(t) = \tilde{\theta}^T(t)\omega(t) = \omega^T(t)\tilde{\theta}(t) \tag{26}$$

Differentiate (25) once to get

$$\frac{dT^{-1}(t)}{dt} = -\lambda(t)T^{-1}(t) + \omega(t)\omega^T(t) \tag{27}$$

From $T(t) * T^{-1}(t) = I$, it follows that

$$\dot{T}(t) = \lambda(t)T(t) - T(t)\omega(t)\omega^T(t)T(t) \tag{28}$$

In summary, the AGC power prediction and parameter identification algorithms are given by

$$\hat{p}(t) = \hat{\theta}^T \omega(t) \tag{29}$$

$$\dot{\hat{\theta}}(t) = -T(t)\omega(t)e(t) \tag{30}$$

$$\dot{T}(t) = \lambda(t)T(t) - T(t)\omega(t)\omega^T(t)T(t) \tag{31}$$

where $\lambda(t)$ is from (21).

Remark 1 In the algorithm (29)-(31), λ_0 and k_0 are predefined parameters representing the maximum forgetting rate and the bound of the gain matrix, respectively. A larger λ_0 results in faster forgetting of historical data, enabling rapid parameter tracking but increasing susceptibility to noise; conversely, a smaller λ_0 yields smoother and more stable estimates at the cost of slower adaptation. The magnitude of the gain matrix is primarily governed by k_0, which must satisfy $k_0 \ge \| T(0)\|$ to ensure $\lambda(t) \ge 0$.

Next, we will show the boundedness of the gain matrix $T(t)$.

Proposition 2 If $\omega(t)$ is persistent excitation, then there exist some positive constants k_1, k_2 and λ_1 such that

$$k_2 I \le T(t) \le k_1 I, \lambda(t) \ge \lambda_1 \tag{32}$$

Proof 2

Substitute (21) into (27) to get

$$\frac{dT^{-1}(t)}{dt} = -\lambda_0 T^{-1}(t) + \frac{\lambda_0}{k_0} \| T(t)\| T^{-1}(t) + \omega(t)\omega^T(t) \tag{33}$$

which when integrated from 0 to t, it follows that

$$T^{-1}(t) = T^{-1}(0)e^{-\lambda_0 t} + \int_0^t e^{-\lambda_0 (t-r)} \left[\frac{\lambda_0}{k_0} \| T(r)\| T^{-1}(r) + \omega(r)\omega^T(r) \right] dr \tag{34}$$

Using $\| T(r)\| T^{-1}(r) \ge I$, it further follows that

$$T^{-1}(t) \ge (T^{-1}(0) - k_0^{-1} I)e^{-\lambda_0 t} + k_0^{-1} I + \int_0^t e^{-\lambda_0 (t-r)} \omega(r)\omega^T(r) dr \tag{35}$$

When $t \ge \delta$, $t - r < \delta$, and if $\omega(t)$ is persistent excitation, then there exists a $\alpha_1 > 0$ such that $\int_0^t \omega(r)\omega^T(r) dr \ge \alpha_1 I$, therefore

$$\int_0^t e^{-\lambda_0 (t-r)} \omega(r)\omega^T(r) dr > e^{-\lambda_0 \delta} \alpha_1 I \tag{36}$$

Substitute (36) into (35), and using $\| T(0)\| \le k_0$ it follows that $T^{-1}(t) \ge (k_0^{-1} + e^{-\lambda_0 \delta} \alpha_1) I$ and then

$$T(t) \le k_1 I, k_1 = \frac{k_0}{1 + k_0 e^{-\lambda_0 \delta} \alpha_1} < k_0 \tag{37}$$

Substitute (37) into (21) to get

$$\lambda(t) = \frac{\lambda_0}{k_0} \left(k_0 - \| T(t)\| \right) \ge \frac{\lambda_0 k_0 \alpha_1 e^{-\lambda_0 \delta}}{1 + k_0 \alpha_1 e^{-\lambda_0 \delta}} \square \lambda_1 > 0 \tag{38}$$

Substitute (38) into (27) to get

$$\frac{dT^{-1}(t)}{dt} \le -\lambda_1 T^{-1}(t) + \omega(t)\omega^T(t) \tag{39}$$

which is integrated from 0 and t to get

$$\begin{aligned} T^{-1}(t) &\le T^{-1}(0)e^{-\lambda_1 t} + \int_0^t e^{-\lambda_1 (t-\tau)}\omega(\tau)\omega^T(\tau)d\tau \\ &\le T^{-1}(0) + \int_0^t e^{-\lambda_1 (t-\tau)}\omega(\tau)\omega^T(\tau)d\tau \end{aligned} \tag{40}$$

where $\int_0^t e^{-\lambda_1 (t-\tau)}\omega(\tau)\omega^T(\tau)d\tau$ is the output of the following filter

$$\dot{M} + \lambda_1 M = \omega(t)\omega^T(t), M(0) = 0 \tag{41}$$

When $\omega(t)$ is persistent excitation, then there exists a positive constant k_2 such that $T(t) \ge k_2 I$.

Finally, we will show the convergence of the parameter estimation error.

Proposition 3

If $\omega(t)$ is persistent excitation, then $\hat{\theta}$ will converge to θ exponentially in the case of constant θ; and converge to a small neighborhood around the origin exponentially in the case of varying θ.

Proof 3

From (26), (27) and (30) it follows that

$$\begin{aligned} \frac{d[T^{-1}(t)\tilde{\theta}]}{dt} &= \frac{d[T^{-1}(t)]}{dt}\tilde{\theta} + T^{-1}(t)\frac{d\tilde{\theta}}{dt} \\ &= -\lambda(t)T^{-1}(t)\tilde{\theta} + \omega\omega^T\tilde{\theta} - T^{-1}(t)\dot{\theta} - \omega e \\ &= -\lambda(t)T^{-1}(t)\tilde{\theta} - T^{-1}(t)\dot{\theta} \end{aligned} \tag{42}$$

In the case of constant θ, $\dot{\theta} = 0$, and the equality above can be written as

$$\frac{d[T^{-1}(t)\tilde{\theta}]}{dt} = -\lambda(t)T^{-1}(t)\tilde{\theta} \le -\lambda_1 T^{-1}(t)\tilde{\theta} \tag{43}$$

which is integrated to get $T^{-1}(t)\tilde{\theta} \le e^{-\lambda_1 t}T^{-1}(0)\tilde{\theta}(0)$, hence $\tilde{\theta} \le e^{-\lambda_1 t}T(t)T^{-1}(0)\tilde{\theta}(0)$. From (32), the parameter estimation error $\tilde{\theta}$ will converge to zero with the rate λ_1.

In the case of varying θ, it is assumed that $\|\dot{\theta}\| \le c_\theta$ which when combined with Proposition 1, it follows $\|T^{-1}(t)\dot{\theta}\|$ is bounded and then the parameter estimation error $\tilde{\theta}$ will converge to a small neighborhood of zero with the rate λ_1.

By comparing the standard LS method with the BGF method, it is known that the BGF method is also suitable for the case where the parameter vector θ is varying.

4. Simulation Validation

In this section, simulations are carried out using one-month AGC commands and actual operation data from a 330 MW thermal power unit in a certain power plant. The power command and the unit's AGC response curve for the first 30,000 seconds is presented in Fig.4.

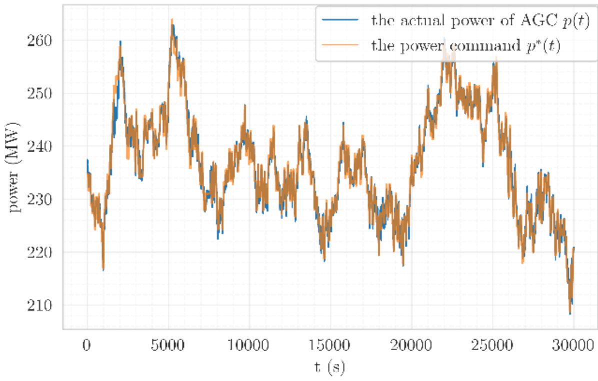

Fig. 4 The actual AGC command and the actual output response curve of a 330MW thermal power unit in a certain power plant

Based on experience and the calibrated technical parameters of the unit, the nominal values of the model parameters are set as $\omega_{n0} = 0.02$ and $\xi_0 = 0.53$. The initial values of adaptive parameters are set as $T(0) = \mathbf{I}$ and $\hat{\theta}(0) = \mathbf{0}$.

Here the average sum of squared deviations serves as a quantitative index to evaluate the identification effect and is calculated as follows [19]:

$$F = \frac{\sum_{t=1}^{m}\left(\hat{p}(t) - p(t)\right)^2}{m} \tag{44}$$

where, t is the sampling time; $p(t)$ represents the output power value of the actual response characteristic curve of the unit at time t; $\hat{p}(t)$ represents the corresponding power estimate at time t; and m is the number of sampling points.

It is shown that power command adjustments are predominantly within the 0~15 MW range according to the statistical analysis of actual AGC data from the 330 MW thermal unit used in our simulations. To systematically evaluate the adaptability of the proposed method under varying conditions, we divide this range into three representative intensity levels: 0~5 MW (low), 6~10 MW (medium), and 11~15 MW (high). For each level, both upward and downward regulation directions are considered, resulting in six distinct operating scenarios:

case 1. Regulation amplitude of 0~5 MW, upward direction; specifically, a data segment with an adjustment magnitude of approximately 3 MW and a duration of about 160 seconds was selected from the aforementioned one-month thermal power dataset in Fig.4.

case 2. Regulation amplitude of 0~5 MW, downward direction; specifically, a data segment with an adjustment magnitude of approximately 3 MW and a duration of about 160 seconds was selected from the aforementioned one-month thermal power dataset in Fig.4.

case 3. Regulation amplitude of 6~10 MW, upward direction; specifically, a data segment with an adjustment magnitude of approximately 8 MW and a duration of about 120 seconds was selected from the aforementioned one-month thermal power dataset in Fig.4.

case 4. Regulation amplitude of 6~10 MW, downward direction; specifically, a data segment with an adjustment magnitude of approximately 9 MW and a duration of about 120 seconds was selected from the aforementioned one-month thermal power dataset in Fig.4.

case 5. Regulation amplitude of 11~15 MW, upward direction; specifically, a data segment with an adjustment magnitude of approximately 11 MW and a duration of about 80 seconds was selected from the aforementioned one-month thermal power dataset in Fig.4.

case 6. Regulation amplitude of 11~15 MW, downward direction. specifically, a data segment with an adjustment magnitude of approximately 11 MW and a duration of about 80 seconds was selected from the aforementioned one-month thermal power dataset in Fig.4.

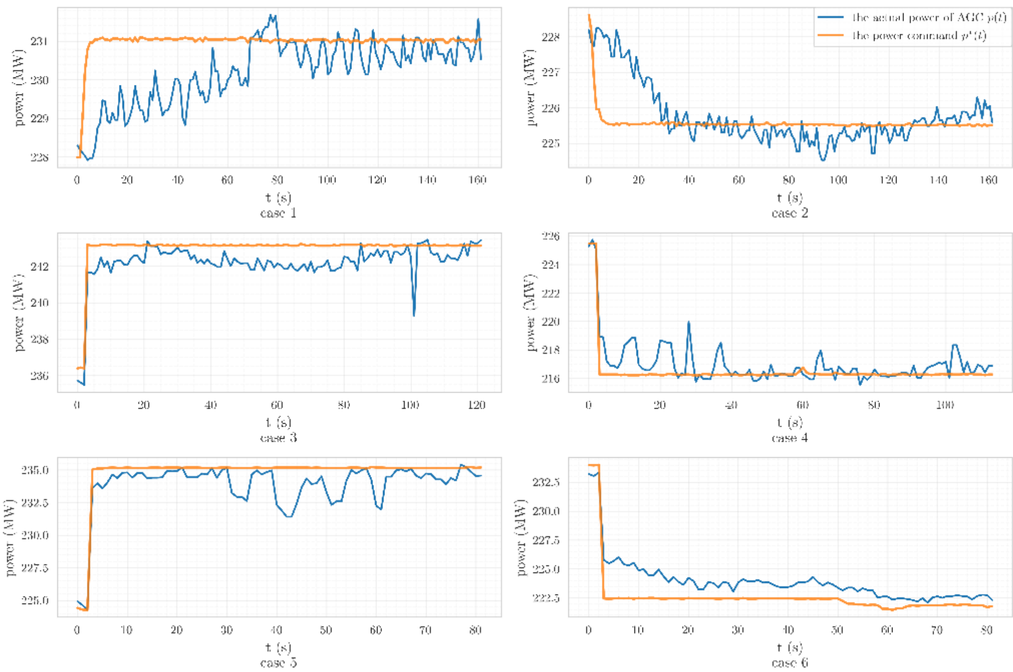

Fig. 5 Curves of the actual power of AGC and the power command in the six cases

We then conduct comparative simulations between the proposed BGF algorithm and the standard LS algorithm in all six scenarios, thereby thoroughly validating the effectiveness and robustness of the proposed approach across different regulation intensities and directions.
The curves of actual power of AGC and the power command under the six cases are shown in Fig.5; the curves of estimated parameter $\hat{\theta}$ using the BGF algorithm and the LS algorithm in the six cases are shown in Fig.6:

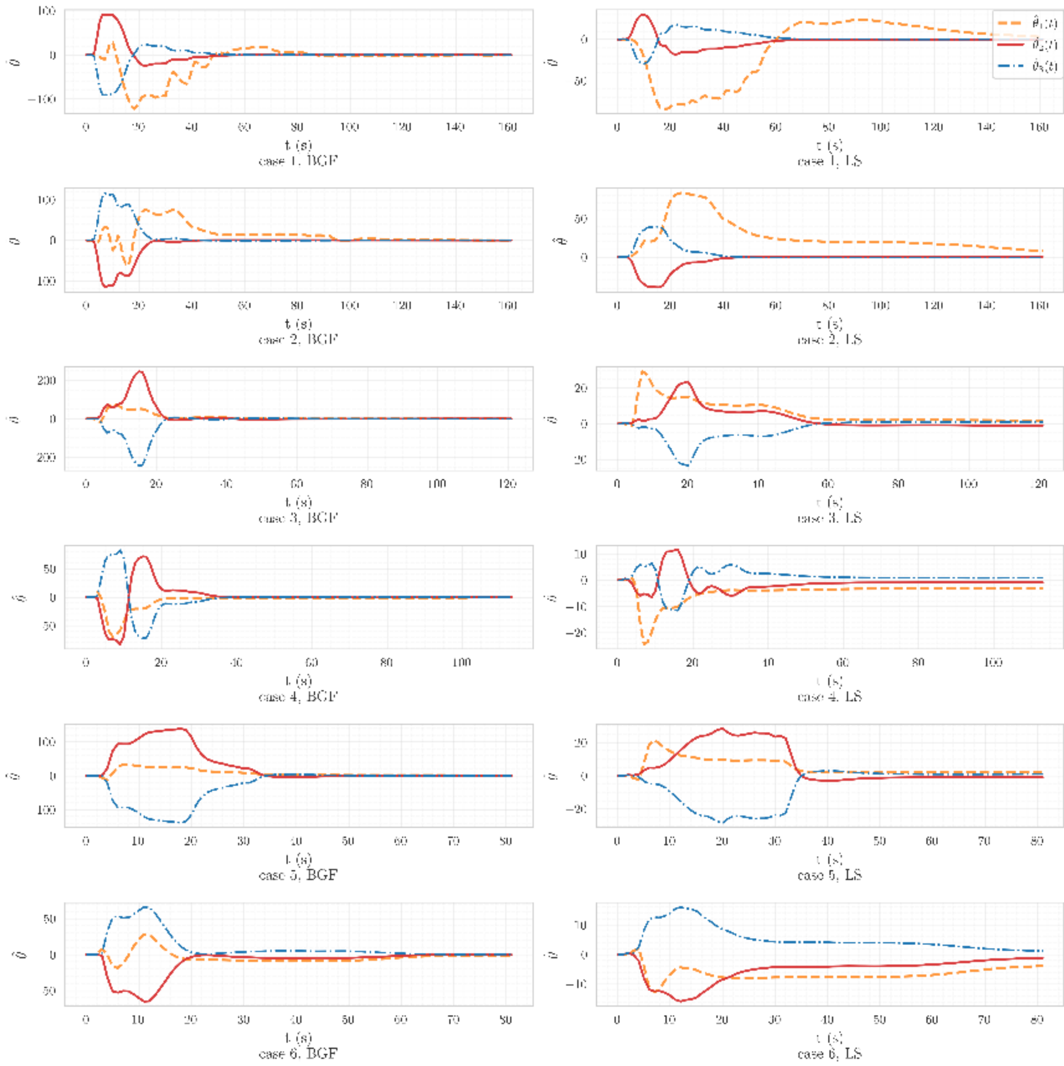

Fig. 6 Curves of parameter estimate $\hat{\theta}$ using the BGF algorithm and the LS algorithm in the six cases

The curves of power prediction error e using the BGF algorithm and the LS algorithm in the six cases are shown in Fig.7; the curve of forgetting factor λ in BGF algorithm in the six cases are presented in Fig.8.

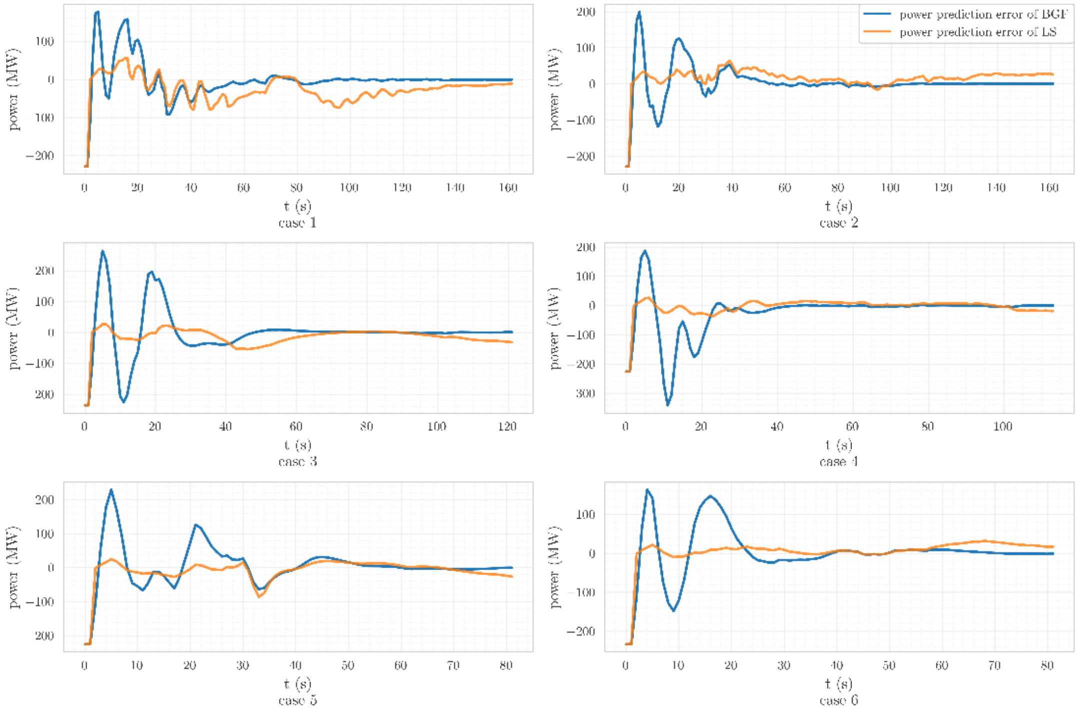

Fig. 7 Curves of power prediction error e in the six cases

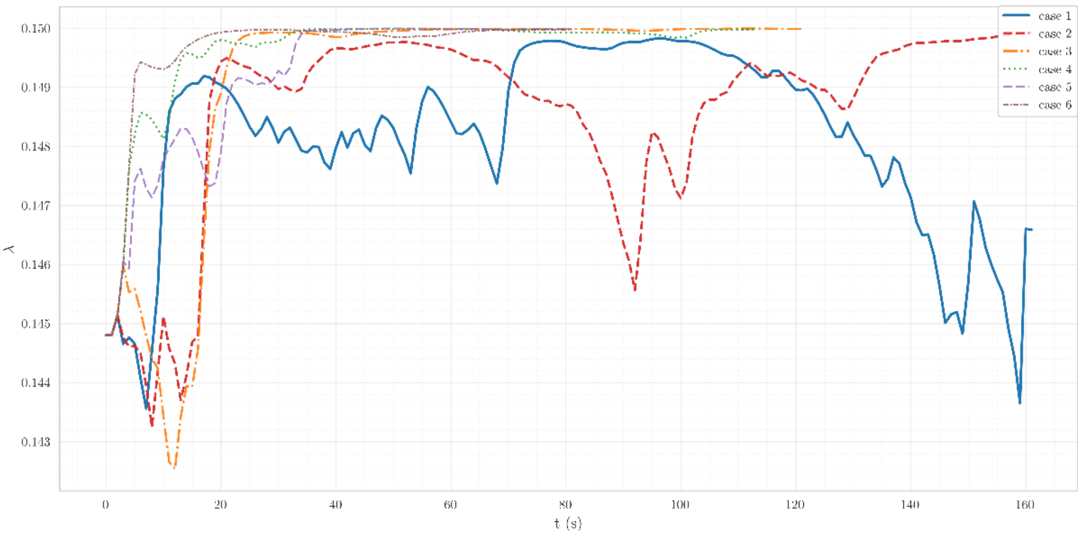

Fig. 8 Curves of forgetting factor λ of BGF algorithm in the six cases

According to (38), the average sum of squared deviations of the BGF algorithm and the LS algorithm are listed in Table 1.

Table 1

The average sum of squared deviations of the BGF algorithm and the LS algorithm

Case Number	BGF	LS
1	23.83	1246.54
2	7.44	328.64
3	7.87	241.45
4	4.47	87.58
5	10.99	163.07
6	28.10	530.56

By comparison, the proposed BGF method has clearly a better performance on parameter estimation and output power prediction.

5. Conclusion

This paper constructs a new adaptive model for secondary frequency regulation of thermal power units, to circumvent the shortcomings of the existing mechanism models. Through the analysis of the thermal power unit's historical operating data, a second-order system is used to model the secondary frequency regulation response characteristics and its parameters are identified with the BGF method. Then a comparison simulation is conducted where the proposed BGF method and standard LS method are respectively adopted for six cases. The simulation results show that the regulation performance of the proposed model is closer to the actual output of the unit, and the average sum of squared deviations is smaller, which fully verifies the superiority of the proposed model.

While the proposed second-order linear model effectively captures the dominant dynamics under large-magnitude AGC commands in "Boiler-Follow" mode, it possesses inherent limitations. It omits explicit representations of critical operational constraints and nonlinearities, such as command deadbands, hard ramping rate limits, and the distinct dynamics between "Boiler-Follow" and "Turbine-Follow" strategies. To address these gaps, future work will prioritize two directions: first, incorporating saturation and dead zone blocks to precisely depict unit behavior across the full range of AGC command amplitudes and operational modes; second, integrating real-time data on the unit's active control mode and ramping limits into the model structure to enhance its adaptability and predictive accuracy.

REFERENCES

[1] *Z. Hu, K. Liu, G. Yu, Y. Shi,* Frequency characteristic analysis of power system considering deep peak load regulation and renewable energy injection, 2021 6th Asia Conference on Power

and Electrical Engineering (ACPEE), Chongqing, China, IEEE, pp. 1578-1582, 2021. Doi: 10.1109/ACPEE51499.2021.9436930

[2] *Z.J. Li, Q.L. Sha, X.R. Yan, G.G. Yan, L. Zhu, Z. Fang, J.W. Li,* A data-driven modeling method for secondary frequency regulation characteristic of thermal power units, Zhejiang Electric Power, Vol. **44**, Iss. 01, pp. 15-23, 2025. Doi: 10.19585/j.zjdl.202501002

[3] *Z. Chen, T. Qin, Z. Zhang, L. Liu,* Study of primary frequency regulation characteristics for thermal power units under deep peak shaving condition, 2021 2nd International Conference on Artificial Intelligence and Computer Engineering (ICAICE), Hangzhou, China, IEEE, pp. 850-854, 2021. Doi: 10.1109/ICAICE54393.2021.00165

[4] *Z. Fang, W.B. Si, D.Y. Wang, L. Zhang, Y.P. Yin, C.P. Li, P. Zhang, G.G. Yan, J.W. Li,* Coordinated control strategy of fire-hybrid-energy-storage system to improve the performance of secondary frequency modulation response, Journal of Global Energy Interconnection, Vol. **8,** Iss. 04, pp. 506-518, 2025. DOI: 10.19705/j.cnki.issn2096-5125.20240202

[5] *F. Hong, W. Ji, Y. Pang, J. Hao, M. Du, F. Fang, J. Liu,* A new energy state-based modeling and performance assessment method for primary frequency control of thermal power plants, Energy, Vol. **276**, pp. 127594, 2023. Doi: 10.1016/j.energy.2023.127594

[6] *Z.Q. Liu, Y. Liu, W.D. Li, H. Yue, Y.X. Su,* Data separation method for primary and secondary frequency regulation response power of thermal power units, Automation of Electric Power Systems, Vol. **47**, Iss. 16, pp. 132-141, 2023. Doi: 10.7500/AEPS20230218001

[7] *Y. Xie, S. Ma, J. Shen, X. Tang, L. Zheng,* Frequency transient analytic analysis considering heat storage dynamic of thermal unit in interconnected power system, Energy Reports, Vol. **13**, pp. 2082-2094, 2025. Doi: 10.1016/j.egyr.2025.01.010

[8] *K. Lin, T. Su, F. Wu, W. Xiang, L. Shi, Y. Li,* An adaptive model predictive control based control strategy of BESS to improve AGC performance of thermal power plant, IEEE Access, Vol. **13**, pp. 99816-99825, 2025. Doi: 10.1109/ACCESS.2025.3573749

[9] *R. Zhang, X. Ren, Z. Liu, Z. Bie, and C. Chen*, Distributed cooperative secondary frequency control for power system penetrated with renewable energy sources and energy storage with communication time delays, International Journal of Electrical Power & Energy Systems, Vol. **164**, pp. 110411, 2025. https://doi.org/10.1016/j.ijepes.2024.110411

[10] *X. Fang, H. Yuan, and J. Tan,* Secondary frequency regulation from variable generation through uncertainty decomposition: An economic and reliability perspective, IEEE Transactions on Sustainable Energy, Vol. **12**, Iss. 4, pp. 2019–2030, 2021. DOI: 10.1109/TSTE.2021.3076758

[11] *Y. Wen, W. Li, G. Huang, and X. Liu,* Frequency dynamics constrained unit commitment with battery energy storage, IEEE Transactions on Power Systems, Vol. **31**, Iss. 6, pp. 5115–5125, 2016. DOI: 10.1109/TPWRS.2016.2521882

[12] *Q. Zhang, H. Tang, Z. Wang, X. Wu, and K. Lv,* Flexible selection framework for secondary frequency regulation units based on learning optimisation method, International Journal of Electrical Power & Energy Systems, Vol. **142**, pp. 108175, 2022. https://doi.org/10.1016/j.ijepes.2022.108175

[13] *S. Zhang, H. Liu, F. Wang, T. Yan, K. Wang,* Secondary frequency control strategy for BESS considering their degree of participation, Energy Reports, Vol. **6**, Iss. 9, pp. 594-602, 2020. Doi: 10.1016/j.egyr.2020.11.183

[14] *B. Yang, L. Weng, Y. Li, Y. Zhang, C. Zhou,* Research on coordinated control strategy of energy storage participating in primary frequency regulation considering frequency deviation change

rate, Journal of Physics: Conference Series, Vol. **1750**, pp. 012034, 2021. Doi: 10.1088/1742-6596/1750/1/012034

[15] *J. Patino, J. Espinosa,* Control sensitivity functions of frequency regulation for a one-area power system, 2017 IEEE 3rd Colombian Conference on Automatic Control (CCAC), Cartagena, Colombia, IEEE, pp. 1–6, 2017. Doi: 10.1109/CCAC.2017.8276460

[16] *B.Y. Sun, Z.Q. Liu, S.L. Yang, R. Wang, T.T. Li,* A real-time optimization method of compensation degree for storage coordinated with thermal power unit in AGC, Power System Technology, Vol. **42**, Iss. 02, pp. 426-436, 2018. Doi: 10.13335/j.1000-3673.pst.2017.1466

[17] *F. Zhang, Z. Yang, G. Wang, K. Meng,* Control strategy of hybrid energy storage system to improve AGC performance of thermal generator, 2018 IEEE Innovative Smart Grid Technologies - Asia (ISGT Asia), Singapore, IEEE, pp. 1299–1304, 2018. Doi: 10.1109/ISGT-Asia.2018.8467771

[18] *L. Zhang, K. Liu, W. Kang,* Research on secondary frequency regulation of thermal power unit assisted by PV storage system, 2023 IEEE/IAS Industrial and Commercial Power System Asia (I&CPS Asia), Chongqing, China, IEEE, pp. 521–525, 2023. Doi: 10.1109/ICPSAsia58343.2023.10294679

[19] *P. Cao, J. Wang, C. Zhang,* Steady-state interval detection and nonlinear modeling for automatic generation control systems, IEEE Access, Vol. **7**, pp. 139592-139600, 2019. Doi: 10.1109/ACCESS.2019.2943166

[20] *J. He, C. Shi, T. Wei, D. Jia,* Stochastic model predictive control of hybrid energy storage for improving AGC performance of thermal generators, IEEE Transactions on Smart Grid, Vol. **13**, Iss. 01, pp. 393-405, 2022. Doi: 10.1109/TSG.2021.3111610

[21] *Z. Tian, J. Yuan, L. Xu,* Modeling of drum boiler-turbine unit and the model-based coordinated control strategy, 2016 35th Chinese Control Conference (CCC), Chengdu, China, IEEE, pp. 3327-3332, 2016. Doi: 10.1109/ChiCC.2016.7553869

[22] *W. Tan, F. Fang, L. Tian, C. Fu, J. Liu,* Linear control of a boiler–turbine unit: analysis and design, ISA Transactions, Vol. **47**, Iss. 02, pp. 189-197, 2008. Doi: 10.1016/j.isatra.2007.02.009

[23] *T. O. Hodson, T. M. Over, S. S. Foks,* Mean squared error, deconstructed, Journal of Advances in Modeling Earth Systems, Vol. **13**, Iss. 12, pp. e2021MS002681, 2021. Doi: 10.1029/2021MS002681